SUPERCONDUCTIVITY

Magnetic field–induced pair density wave state in the cuprate vortex halo

S. D. Edkins[1,2,3], A. Kostin[1], K. Fujita[1,4], A. P. Mackenzie[3,5], H. Eisaki[6], S. Uchida[7], Subir Sachdev[8], Michael J. Lawler[1,9], E.-A. Kim[1], J. C. Séamus Davis[1,4,10,11]*, M. H. Hamidian[1,8]*

High magnetic fields suppress cuprate superconductivity to reveal an unusual density wave (DW) state coexisting with unexplained quantum oscillations. Although routinely labeled a charge density wave (CDW), this DW state could actually be an electron-pair density wave (PDW). To search for evidence of a field-induced PDW, we visualized modulations in the density of electronic states $N(r)$ within the halo surrounding $Bi_2Sr_2CaCu_2O_8$ vortex cores. We detected numerous phenomena predicted for a field-induced PDW, including two sets of particle-hole symmetric $N(r)$ modulations with wave vectors Q_P and $2Q_P$, with the latter decaying twice as rapidly from the core as the former. These data imply that the primary field-induced state in underdoped superconducting cuprates is a PDW, with approximately eight CuO_2 unit-cell periodicity and coexisting with its secondary CDWs.

Theory predicts that Cooper pairs with finite center-of-mass momentum $\boldsymbol{p} = \hbar\boldsymbol{Q_P}$ (where $\hbar$ is Planck's constant h divided by 2π) should form a state in which the density of pairs modulates spatially at wave vector $\boldsymbol{Q_P}$ (*1*, *2*). In the phase diagram of underdoped cuprates, such a "pair density wave" (PDW) state (*3*–*5*), generated by strong local electron-electron interactions (*6*–*11*), is anticipated to be another principal state, along with uniform superconductivity. Numerous experimental observations may be understood in that context. For example, although intraplanar superconductivity appears in $La_{2-x}Ba_xCuO_4$ at relatively high temperatures, interplanar superconductivity is strongly frustrated (*12*), which is consistent with the existence of orthogonal unidirectional PDW states in each sequential CuO_2 plane (*3*, *13*, *14*). Moreover, the measured momentum-space electronic structure of the cuprate pseudogap phase is consistent with predictions that are based on a biaxial PDW (*4*). Reported breaking of time-reversal symmetry could be caused by a PDW with inversion breaking (*15*–*18*). The field-induced momentum-space reconstruction and quantum oscillation phenomenology are potentially the consequences of a PDW state (*19*–*21*), although this view is not universal (*22*). At the highest fields, strong diamagnetism in torque magnetometry (*23*) and supercurrents in dc transport might also be understood as being due to a field-induced PDW state. Most recently, scanned Josephson tunneling microscopy allows direct visualization of cuprate pair density modulations (*24*). Taken together, these studies indicate that a fundamental PDW state may exist in underdoped cuprates, with the most common model invoked being an eight unit-cell ($8a_0$) periodic modulation of the electron-pair condensate.

Such a PDW state clearly does not predominate at low temperature in zero magnetic field, where global d-wave superconductivity is robust. However, suppression of the superconductivity by high magnetic fields generates a peculiar DW state (*25*–*32*) along with exotic quantum oscillation phenomenology (*33*, *34*). For type II superconductors in general, application of a magnetic field generates quantized vortices. At the vortices of a conventional d-wave superconductor, the four zeros in the energy gap should generate a slowly decaying, star-shaped, zero-energy resonance oriented along the nodal (±1, ±1) directions. For cuprates, however, strong $N(\boldsymbol{r}, E)$ modulations oriented along (1, 0); (0, 1) directions have long been observed in the "halo" region that surrounds the cuprate vortex core (*35*–*38*). Many theories hypothesize that this phenomenon is a field-induced DW (*5*, *39*–*43*), and some hypothesize that it is not a conventional CDW but a PDW (*4*, *5*, *22*, *43*). This is a fundamental distinction because the PDW and CDW are extremely different states in terms of their broken symmetries and many-body wave functions. Thus, to determine whether the primary DW state induced by magnetic field in superconducting cuprates is a PDW has recently become an urgent research challenge.

To search for evidence of such a state, we studied the field-induced modulations of the density of electronic states $N(\boldsymbol{r}, E)$ within the halo surrounding quantized vortex cores (*35*–*38*). Any periodic modulations of electronic structure can be described by $A(\boldsymbol{r}) = AF(\theta)\cos(\boldsymbol{Q}\cdot\boldsymbol{r} + \phi_0)$, where $A(\boldsymbol{r})$ represents the modulating electronic degree of freedom with amplitude A, $\boldsymbol{Q}$ is the wave vector, and $F(\theta)$ is the modulation form factor defined in terms of the angle θ from the (1, 0) axis. An s-symmetry form factor $F_S(\theta)$ is even under 90° rotations, whereas a d-wave form factor is $F_d(\theta)$ is odd. Following (*5*), the order parameters we considered are those of homogenous d-wave superconductivity $\Delta(\boldsymbol{r}) = F_{SC}\Delta_{SC}$, with $F_{SC} = F_d$, and that of a PDW $\Delta_{PD}(r) = F_P\Delta_P^Q(e^{i\boldsymbol{Q_P}\cdot\boldsymbol{r}} + e^{-i\boldsymbol{Q_P}\cdot\boldsymbol{r}})$, with wave vector $\boldsymbol{Q_P}$ and either an F_s or F_d type of form factor [(*44*), section 1]. A field-induced PDW may be identified from Ginzburg-Landau (GL) analysis (*5*, *22*, *43*) of the interactions between these two order parameters within vortex halos—regions of suppressed but nonzero superconductivity that surround vortex cores (Fig. 1A). Given a generic GL free-energy density of the form

$$\mathcal{F}_{A-SC} = \mathcal{F}(\Delta_{SC}) + \mathcal{F}(\Delta_A) + u_1|\Delta_A|^2|\Delta_{SC}|^2 \quad (1)$$

where $\mathcal{F}(\Delta_{SC})$ and $\mathcal{F}(\Delta_A)$ are the free-energy densities of a superconductor and of an alternative repulsively coupled ($u_1 > 0$) state Δ_A, the observation of coexistence of Δ_A with Δ_{SC} within the vortex halo [(*44*), section 2] means that the two ordered states are almost energetically degenerate (*39*). Such a near degeneracy occurs naturally between a superconductor Δ_{SC} and a PDW Δ_P^Q that are made up of the same electron pairs. In this case, allowed $N(\boldsymbol{r})$ modulations generated by interactions between Δ_{SC} and Δ_A can be found from products of these order parameters that transform as density-like quantities. For example, the product of PDW and uniform SC order parameters

$$A_{\boldsymbol{Q_P}} \propto \Delta_P^Q\,\Delta_{SC}^* \Rightarrow N(\boldsymbol{r}) \propto \cos(\boldsymbol{Q_P}\cdot\boldsymbol{r}) \quad (2)$$

results in $N(\boldsymbol{r})$ modulations at the PDW wave vector $\boldsymbol{Q_P}$. The product of a robust PDW with itself

$$A_{\boldsymbol{2Q_P}} \propto \Delta_P^Q\Delta_P^{-Q*} \Rightarrow N(\boldsymbol{r}) \propto \cos(2\boldsymbol{Q_P}\cdot\boldsymbol{r}) \quad (3)$$

produces $N(\boldsymbol{r})$ modulations occurring at $2\boldsymbol{Q_P}$. Thus, a key signature of a field-induced PDW with wave vector $\boldsymbol{Q_P}$ in cuprate vortex halos (Fig. 1A) would be coexistence of two sets of $N(\boldsymbol{r})$ modulations at $N(\boldsymbol{r})$ and at $2\boldsymbol{Q_P}$ within each halo (Fig. 1B) (*5*, *22*, *43*).

Within GL theory, substantial further information can be extracted from measured rates of decay of the induced $N(\boldsymbol{r})$ modulations away from the vortex center and from the form factors of these modulations within the vortex halo. For a field-induced PDW, the $N(\boldsymbol{r}, E)$ modulations at $2\boldsymbol{Q_P}$ should decay with distance from the core at twice the rate as those at $\boldsymbol{Q_P}$. This is because if $\Delta_P^Q = \Delta_P^Q(|\boldsymbol{r}| = 0)e^{-|r|/\xi}$, then $\Delta_P^Q\Delta_P^{-Q*}$ decays with $|r|$ at twice the rate of $\Delta_P^Q\Delta_{SC}^*$ (Fig. 1B). Current theory (*22*, *43*) indicates that if the $N(\boldsymbol{r}, E)$ modulations at $\boldsymbol{Q_P}$ caused by $\Delta_P^Q\Delta_{SC}^*$

[1]Laboratory of Atomic and Solid State Physics, Department of Physics, Cornell University, Ithaca, NY 14853, USA. [2]Department of Applied Physics, Stanford University, Stanford, CA 94305, USA. [3]School of Physics and Astronomy, University of St. Andrews, Fife KY16 9SS, Scotland. [4]Condensed Matter Physics Department, Brookhaven National Laboratory, Upton, NY, USA. [5]Max-Planck Institute for Chemical Physics of Solids, D-01187 Dresden, Germany. [6]Institute of Advanced Industrial Science and Technology, Tsukuba, Ibaraki 305-8568, Japan. [7]Department of Physics, University of Tokyo, Bunkyo-ku, Tokyo 113-0033, Japan. [8]Department of Physics, Harvard University, Cambridge, MA 02138, USA. [9]Department of Physics and Astronomy, Binghamton University, Binghamton, NY 13902, USA. [10]Department of Physics, University College Cork, Cork T12R5C, Ireland. [11]Clarendon Laboratory, Oxford University, Oxford, OX1 3PU, UK.
*Corresponding author. Email: jcdavis@ccmr.cornell.edu (J.C.S.D.); mhh32@cornell.edu (M.H.H.)

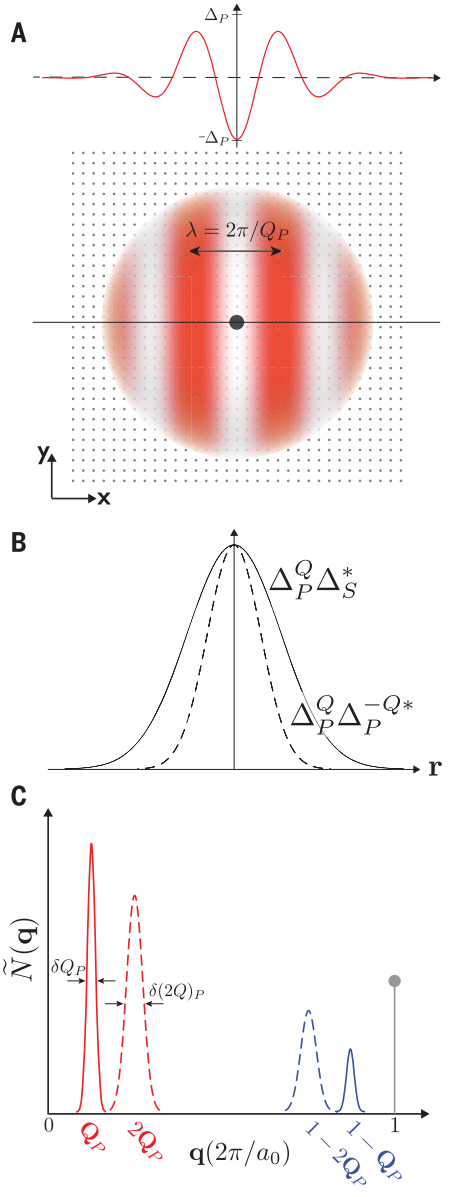

Fig. 1. Schematic of field-induced unidirectional $8a_0$ PDW. (**A**) Diagram of the halo region (gray) surrounding the vortex core (black) of a cuprate superconductor (SC). The CuO_2 plane orientation and Cu–Cu periodicity are indicated by using a dot for each Cu site. Within the halo, a unidirectional PDW modulation along the *x* axis with periodicity $8a_0$, characterized by an order parameter $\Delta_P^Q(\boldsymbol{r})$ shown as red curve in the top graph, is indicated schematically with red shading. (**B**) Solid curve indicates envelope containing nonzero amplitude $\Delta_P^Q \Delta_{SC}^*$ of the $N(\boldsymbol{r})$ modulations caused by the interaction between the SC and PDW order parameters, plotted along the fine horizontal line in (A) through the vortex core. Dashed curve indicates the envelope containing nonzero amplitude $\Delta_P^Q \Delta_P^{-Q*}$ of the $N(\boldsymbol{r})$ modulations caused by PDW itself, plotted along the same fine line. For clarity, we ignore the small region (less than 1 nm) at the core where $\Delta_P^Q \Delta_{SC}^*$ must rise from zero as Δ_{SC} does. (**C**) Within a GL model, if the field-induced PDW has a pure *d*-symmetry form factor, $F_P = F_d$, then two sets of $N(\boldsymbol{r})$ modulations should appear together. The first is $N(\boldsymbol{r}) \propto \cos(\boldsymbol{Q_P} \cdot \boldsymbol{r})$ caused by $\Delta_P^Q \Delta_S^*$ and indicated in $\tilde{N}(\boldsymbol{q})$ [the Fourier transform of $N(\boldsymbol{r})$] with a solid red curve. The second $N(\boldsymbol{r}) \propto \cos(2\boldsymbol{Q_P} \cdot \boldsymbol{r})$ caused by $\Delta_P^Q \Delta_P^{-Q*}$ is indicated in $\tilde{N}(\boldsymbol{q})$ with a dashed red curve. The decay length for the $2\boldsymbol{Q_P}$ modulation should be half that of the $\boldsymbol{Q_P}$ modulation, meaning that the linewidth $\delta(2Q)_P$ of the $2\boldsymbol{Q_P}$ modulation (dashed red) should be twice that of the $\boldsymbol{Q_P}$ modulation, δQ_P (solid red). If the PDW has a pure *s*-symmetry form factor, $F_P = F_S$, then a different pair of $N(\boldsymbol{r})$ modulations should appear together. First is $N(\boldsymbol{r}) \propto \cos[(\boldsymbol{Q_B} - \boldsymbol{Q_P}) \cdot \boldsymbol{r}]$, caused by $\Delta_P^Q \Delta_S^*$ (solid blue line), and second $N(\boldsymbol{r}) \propto \cos(2\boldsymbol{Q_P} \cdot \boldsymbol{r})$, caused by $\Delta_P^Q \Delta_P^{-Q*}$ (dashed blue line). Here, $\boldsymbol{Q_B}$ is the Bragg wave vector of the CuO_2 unit cell.

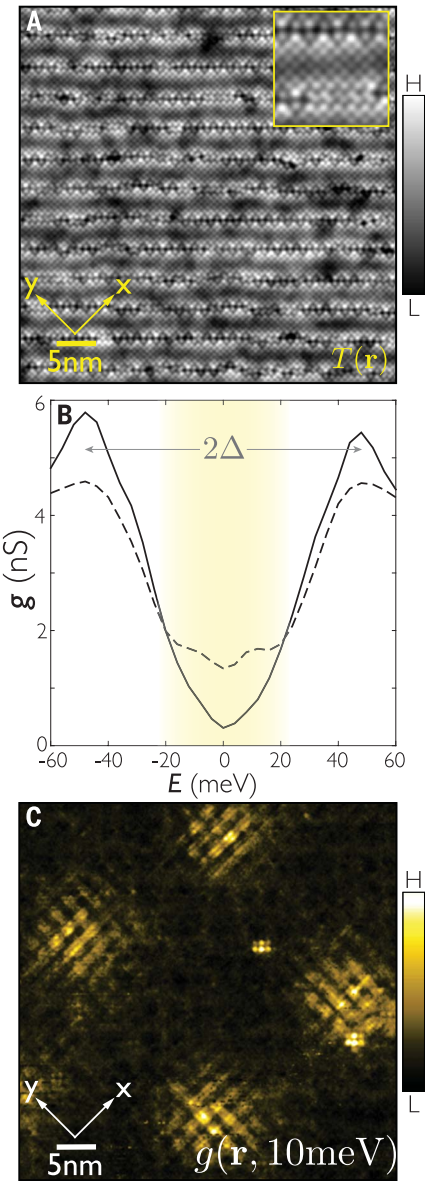

Fig. 2. Four-unit-cell quasiparticle modulations at vortex halos in $Bi_2Sr_2CaCu_2O_8$. (**A**) Topographic image $T(\boldsymbol{r})$ of BiO termination layer of our $Bi_2Sr_2CaCu_2O_8$ sample. The displacement of every specific atomic site in this field of view between zero field and B = 8.25 T was constrained by post processing of all low- and high-field data sets to be less than 10 pm [(*45*), section 3]. (**B**) Measured differential tunnel conductance spectrum $g(\boldsymbol{r}, E = \text{eV}) \equiv dI/dV(\boldsymbol{r}, V)$ showing how to identify the symmetry point of a vortex core (dashed line). The full line shows measured $g(\boldsymbol{r}, E = \text{eV})$ at the identical location in zero field. Yellow-shaded region indicates low-energy Bogoliubov quasiparticle states generated by the vortex. (**C**) Measured $\delta g(\boldsymbol{r}, 12\text{ meV}) = g(\boldsymbol{r}, 12\text{ meV}, B = 8.25\ T) - g(\boldsymbol{r}, 12\text{ meV}, B = 0)$ showing typical examples of the low-energy Bogoliubov quasiparticle modulations (*35*–*38*) within halo regions surrounding four vortex cores in $Bi_2Sr_2CaCu_2O_8$.

exhibit *s*-symmetry form factor (F_s), this implies that the PDW order parameter Δ_P^Q contains components with *d*-symmetry form factor (F_d), and vice versa [(*44*), section 2]. These studies (*22*, *43*) sustain the original GL approach (*5*) by showing that an $8a_0$ PDW stabilized in the halo of a *d*-wave vortex core does indeed generate both an $8a_0$ and a $4a_0$ periodic charge modulation therein. Overall, because a *d*-symmetry form factor PDW is typically predicted for cuprates (*6*–*11*), its signature within a vortex halo should be two sets of $N(\boldsymbol{r})$ modulations occurring at $\boldsymbol{Q_P}$ and $2\boldsymbol{Q_P}$, both with *s*-symmetry form factor components and with the amplitude of the $2\boldsymbol{Q_P}$ modulation decaying twice as rapidly as that at $\boldsymbol{Q_P}$.

To explore these predictions, we imaged scanning tunneling microscope (STM) tip-sample differential tunneling conductance $dI/dV(\boldsymbol{r}, V) \equiv g(\boldsymbol{r}, E)$ versus bias voltage $V = E/e$ and location $\boldsymbol{r}$ with sub–unit-cell spatial resolution; no scanned Josephson tunneling microscopy (*24*) was involved. We measured slightly underdoped $Bi_2Sr_2CaCu_2O_8$ samples [superconducting transition temperature $T_c \sim 88$K; hole doping $p \sim 17\%$] at temperature T = 2 K. We first measured the $N(\boldsymbol{r}, E)$ at zero field and then at magnetic field B = 8.25 T, in the identical field of view (FOV), using an identical STM tip (*35*). The former was subtracted from the latter to yield the field-induced changes $\delta g(\boldsymbol{r}, E, B) = g(\boldsymbol{r}, E, B) - g(\boldsymbol{r}, E, 0)$, which are related to the field-induced perturbation to the density of states as $\delta N(\boldsymbol{r}, E, B) \propto \delta g(\boldsymbol{r}, E, B)$. This step ensures that the phenomena studied thereafter were only those induced by the magnetic field, with all signatures of the ubiquitous *d*-symmetry form factor DW observed at $B = 0$ (*45*) having been subtracted. Compared with our prior vortex halo studies (*35*), we enhanced the $\boldsymbol{r}$-space resolution using smaller pixels and the $\boldsymbol{q}$-space resolution by using larger FOV (58 by 58 nm), increased the

number of vortices per image, used distortion-corrected sublattice-phase-resolved imaging (*45*), and measured in a far wider energy range $0 < |E| < 80$ meV [(*44*), section 3].

We next identified the location of every vortex halo in $\delta g(\boldsymbol{r}, E, B)$ images using two well-known phenomena: (i) suppression of the superconducting coherence peaks at the vortex symmetry point (Fig. 2B) and (ii) appearance of low-energy periodic conductance modulations (*35*–*38*) surrounding this point. A typical symmetry-point spectrum of the superconducting vortex where maximum suppression of the single-particle coherence peaks occurs is shown in Fig. 2B; these peaks recover very rapidly as a function of radius, so that robust *d*-wave superconductivity signified by full coherence peaks has recovered within a radius of ~1 nm [(*44*), section 4]. At $E = 12$ meV, the typical halo of conductance modulations we detected surrounding each vortex symmetry point (Fig. 2C) was in excellent agreement with previous studies of modulations of low-energy quasiparticles, with $\boldsymbol{q} \approx (\pm 1/4, 0); (0, \pm 1/4)2\pi/a_0$ within the $Bi_2Sr_2CaCu_2O_{8-x}$ vortex halo (*35*–*38*). We focused on a different energy range $25 < |E| < 50$ meV because analysis of our $\delta g(\boldsymbol{r}, E)$ data revealed major changes in this range. In Fig. 3A, we show measured $\delta g(\boldsymbol{r}, 30\text{ meV})$ containing the modulations detected in the halo of each vortex core. Fourier analysis of this $\delta g(\boldsymbol{r}, 30\text{ meV})$ yields $|\tilde{\delta g}(\boldsymbol{q}, 30\text{ meV})|$ and reveals a set of sharp peaks at $\boldsymbol{q} = (\boldsymbol{Q}_P^x; \boldsymbol{Q}_P^y) \approx [(\pm 1/8, 0)(0, \pm 1/8)]2\pi/a_0$, which we label $\boldsymbol{Q_P}$ for reasons explained below (Fig. 3B). Similarly, there is a second set of weaker modulations in $\tilde{\delta g}(\boldsymbol{q}, 30\text{ meV})$ at $\boldsymbol{q} \approx [(\pm 1/4, 0); (0, \pm 1/4)]2\pi/a_0$, which we label $2\boldsymbol{Q_P}$. The $\boldsymbol{r}$-space amplitude envelopes of the $\boldsymbol{Q_P}$ and $2\boldsymbol{Q_P}$ modulations (Fig. 3, C and D) reveal how these field-induced phenomena are confined to the vortex halo regions only. Averaged over all vortices, the measured amplitude $|\tilde{\delta g}(\boldsymbol{q}, 30\text{ meV})|$ plotted along (1, 0) in Fig. 3E discernibly discriminates the $\boldsymbol{Q_P}$ from the $2\boldsymbol{Q_P}$ modulation peaks. Thus, we discovered strong, field-induced modulations of $N(\boldsymbol{r}, E)$, with period approximately $8a_0$ coexisting with weaker modulations of period approximately $4a_0$, along both the (1, 0); (0, 1) directions within every vortex halo. These particle-hole symmetric phenomena exist within the energy range $25 < |E| < 45$ meV [(*44*), section 5].

To evaluate form factor symmetry for these field-induced modulations [(*44*), section 6], we separated each such $\delta g(\boldsymbol{r}, E)$ image into three sublattice images (*46*): $Cu(\boldsymbol{r}, E)$, containing only the measured values of $\delta g(\boldsymbol{r}, E)$ at copper sites, and $O_x(\boldsymbol{r}, E)$ and $O_y(\boldsymbol{r}, E)$, containing only those at the x/y axis oxygen sites. All of the form factors discussed here refer to modulations in $\delta g(\boldsymbol{r}, E, B)$ and are not necessarily those of the order parameter of the field-induced state that generates them. Complex-valued Fourier transforms of the $O_x(\boldsymbol{r}, E)$ and $O_y(\boldsymbol{r}, E)$ sublattice images yield $\tilde{O}_x(\boldsymbol{q}, E)$; $\tilde{O}_y(\boldsymbol{q}, E)$. Then, modulations at any $\boldsymbol{Q}$ having *d*-symmetry form factor F_d generate a peak in $\tilde{D}^{\delta g}(\boldsymbol{q}, E) \equiv \tilde{O}_x(\boldsymbol{q}, E) - \tilde{O}_y(\boldsymbol{q}, E)$ at $\boldsymbol{Q}$, whereas those with *s*-symmetry form factor F_s generate a peak in $\tilde{S}^{\delta g}(\boldsymbol{q}, E) \equiv [\tilde{O}_x(\boldsymbol{q}, E) + \tilde{O}_y(\boldsymbol{q}, E)] + \tilde{Cu}(\boldsymbol{q}, E)$ at $\boldsymbol{Q}$. When we analyzed the data in Fig. 3, A and B, in this way using measured $\tilde{S}^{\delta g}(\boldsymbol{q}, 30\text{ meV})$, the field-induced $\delta g(\boldsymbol{r}, E)$-modulations occurring at $\boldsymbol{q} \approx (\pm Q_P, 0); (0, \pm Q_P)$ and $\boldsymbol{q} \approx (\pm 2Q_P, 0); (0, \pm 2Q_P)$ all exhibited *s*-symmetry form factors (Fig. 3E).

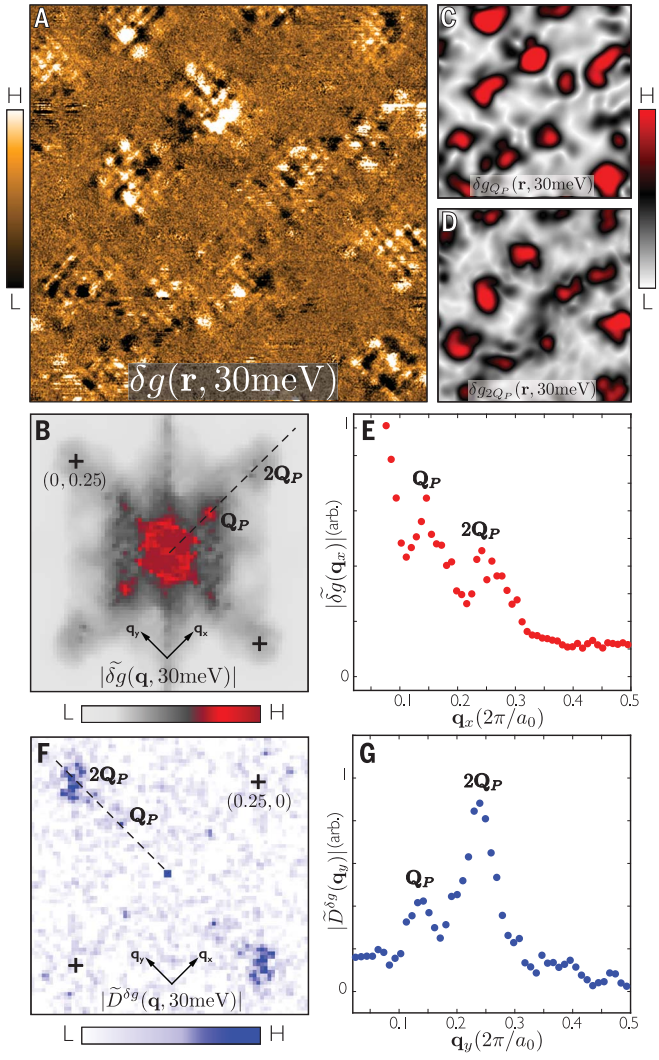

Fig. 3. Field-induced *s*-symmetry form factor modulations within vortex halos. (**A**) Measured field-induced modulations $\delta g(\boldsymbol{r}, 30\text{ meV}) = g(\boldsymbol{r}, 30\text{ meV}, B = 8.25\ T) - g(\boldsymbol{r}, 30\text{ meV}, B = 0)$ in a 58 by 58 nm FOV. The simultaneously measured topographs $T(\boldsymbol{r})$ at $B = 8.25$ T and 0 T are shown in fig. S2 and (*44*), section 3, and demonstrate by the absence of local maxima at $\boldsymbol{q} \approx [(\pm 1/8, 0); (0, \pm 1/8)]2\pi/a_0$ in their Fourier transforms that the setup effect is not influencing observations of $\delta g(\boldsymbol{r}, E)$ modulations at these wave vectors [(*44*), section 5]. (**B**) Amplitude Fourier transform $|\tilde{\delta g}(\boldsymbol{q}, 30\text{ meV})|$ (square root of power spectral density) of $\delta g(\boldsymbol{r}, 30\text{ meV})$ data in (A). The $\boldsymbol{q} = (\pm 1/4, 0); (0, \pm 1/4)2\pi/a_0$ points are indicated with black crosses. Four sharp maxima, indicated by $\boldsymbol{Q_P}$, occur at $\boldsymbol{q} = (\pm 1/8, 0); (0, \pm 1/8)2\pi/a_0$, whereas four broader maxima, indicated by $2\boldsymbol{Q_P}$, occur at $\boldsymbol{q} = (\pm 1/4, 0); (0, \pm 1/4)2\pi/a_0$. (**C**) Measured amplitude envelope of the modulations in $\delta g(\boldsymbol{r}, 30\text{ meV})$ at $\boldsymbol{Q_P}$ showing that they only occur within the vortex halo regions. (**D**) Measured amplitude envelope of the modulations in $\delta g(\boldsymbol{r}, 30\text{ meV})$ at $2\boldsymbol{Q_P}$, showing that they also only occur within the vortex halo regions. (**E**) Measured $|\tilde{\delta g}(\boldsymbol{q}, 30\text{ meV})|$ along (0,0)-(1/2,0) [(B), dashed line], showing the two maxima in the field-induced $N(\boldsymbol{r})$ modulations, occurring at by $\boldsymbol{Q_P} = 0.117 \pm 0.01$ and $2\boldsymbol{Q_P} = 0.231 \pm 0.01$ (Fig. 4, A to D) (**F**) Amplitude Fourier transform of the *d*-symmetry form factor modulations in $N(\boldsymbol{r})$, $|\tilde{D}^{\delta g}(\boldsymbol{q}, 30\text{ meV})|$, derived from measured $\delta g(\boldsymbol{r}, 30\text{ meV})$ data in (A). Again, $\boldsymbol{q} = (\pm 1/4, 0); (0, \pm 1/4)2\pi/a_0$ points are indicated with black crosses. Two maxima, labeled as $\boldsymbol{Q_P}$, occur at $\boldsymbol{q} = (\pm 1/8, 0); (0, \pm 1/8)2\pi/a_0$, whereas two broader maxima, indicated by $2\boldsymbol{Q_P}$ occur at $\boldsymbol{q} = (\pm 1/4, 0); (0, \pm 1/4)2\pi/a_0$, with both sets oriented along the *y* axis. (**G**) Measured $|\tilde{D}^{\delta g}(\boldsymbol{q}, 30\text{ meV})|$ along (0,0)-(1/2,0) [(F), dashed line], showing the maxima in the field induced $N(\boldsymbol{r})$ modulations occurring at $\boldsymbol{Q_P}$ and $2\boldsymbol{Q_P}$. A unidirectional *d*-symmetry form factor change density modulation, as observed extensively in zero field (*46*), would have such characteristics, as would contributions from an *s*-symmetry form factor PDW. These modulations do not appear in Fig. 3 because, in that unprocessed $\delta g(\boldsymbol{r}, E)$ data, they occur at $\boldsymbol{Q} \approx (0, \pm 7/8)2\pi/a_0$ and $\boldsymbol{Q} \approx (0, \pm 3/4)2\pi/a_0$ owing to their *d*-symmetry form factor (Fig. 4, A to D).

However, the measured $\tilde{D}^{\delta g}(\boldsymbol{q}, 30\text{ meV})$ in Fig. 3, F and G, also revealed that weaker *d*-symmetry $\delta g(\boldsymbol{r}, E)$-modulations occur at $\boldsymbol{q} \approx (0, \pm Q_P)$ and $\boldsymbol{q} \approx (0, \pm 2Q_P)$. They too are confined to the vortex halo because the $\boldsymbol{r}$-space amplitude-envelope of the $2\boldsymbol{Q}_P$-modulations in $\tilde{D}^{\delta g}(\boldsymbol{q}, 30\text{ meV})$ is concentrated there.

The overall measured amplitudes of $|\widetilde{\delta g}(\boldsymbol{q}, 30\text{ meV})|$ derived from $\delta g(\boldsymbol{r}, 30\text{ meV})$ in Fig. 3A are shown in Fig. 4, A and B, plotted along the (1,0) and (0,1) directions of the CuO_2 plane. Equivalent cuts of $|\widetilde{\delta g}(\boldsymbol{q}, -30\text{ meV})|$ derived from $\delta g(\boldsymbol{r}, -30\text{ meV})$ data are shown in Fig. 4, C and D. The four maxima at $|\boldsymbol{q}| \approx 1/8$, $|\boldsymbol{q}| \approx 1/4$, $|\boldsymbol{q}| \approx 3/4$, and $|\boldsymbol{q}| \approx 7/8$ associated with field-induced modulations occur in Fig. 4, A to D. The measured form factor of each set of modulations is identified by color code, red indicating *s*-symmetry and blue indicating *d*-symmetry. Although modulations at $|\boldsymbol{q}| \approx 7/8$ and $|\boldsymbol{q}| \approx 3/4$ (Fig. 4, A to D, blue) appear subdominant, they do merit comment. First,

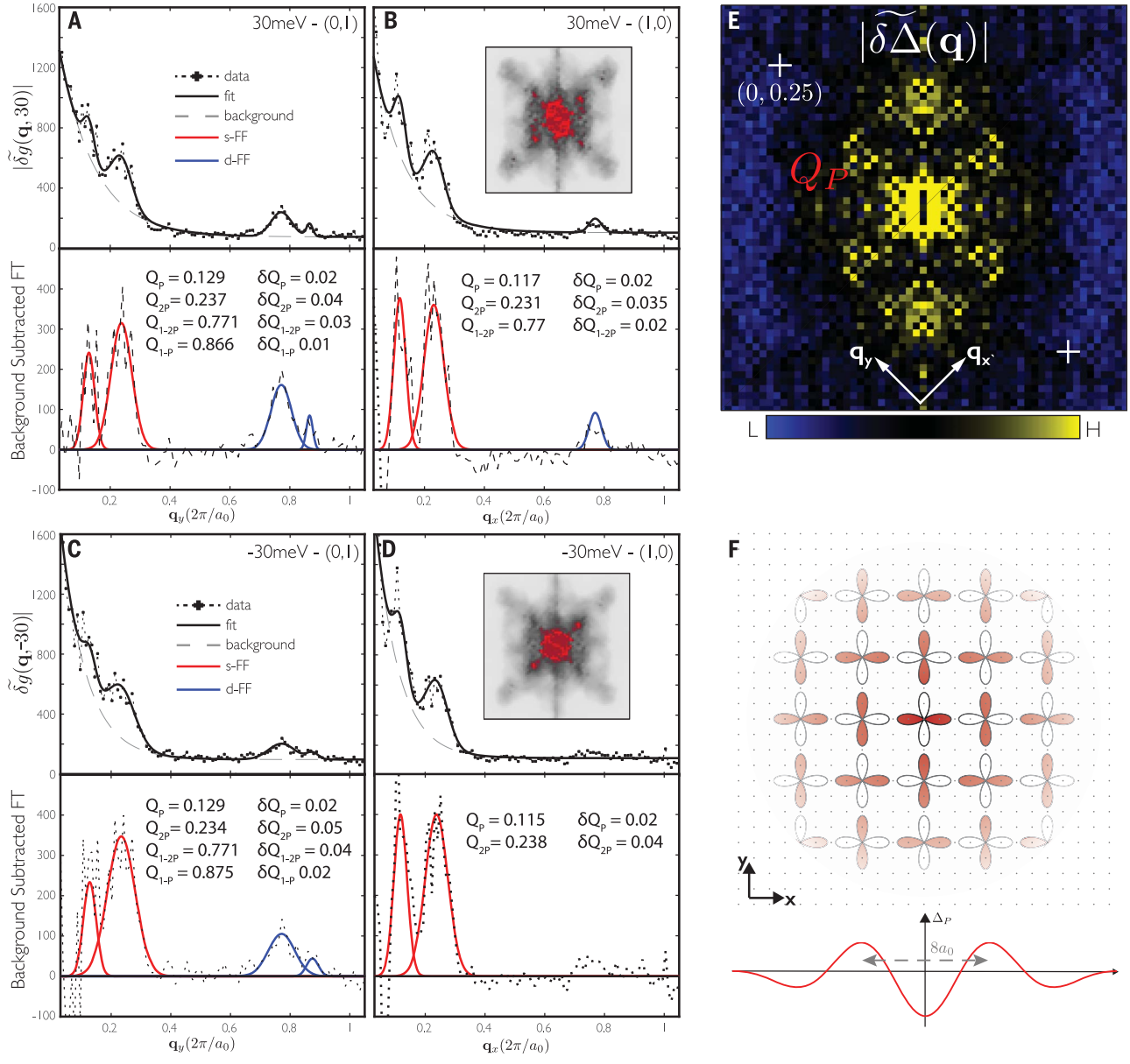

Fig. 4. Field-induced *N*(*r*) modulations indicative of a PDW state in the vortex halo. (**A** and **B**) Amplitude Fourier transform $|\widetilde{\delta g}(\boldsymbol{q}, 30\text{ meV})|$ derived from $\delta g(\boldsymbol{r}, 30\text{ meV})$ data are plotted along two orthogonal axes from (0,0)-(0,1) and (0,0)-(1,0), to reach both Bragg points. All four local maxima, at $\boldsymbol{Q_P}$ and $2\boldsymbol{Q_P}$ from the *s*-symmetry field-induced $N(\boldsymbol{r})$ modulations, plus at $1 - \boldsymbol{Q_P}$ and $1 - 2\boldsymbol{Q_P}$ from the *d*-symmetry field-induced $N(\boldsymbol{r})$ modulations, may be seen. Measurement from these fits of the *q*-magnitude and width δq of the *s*-symmetry peaks at $\boldsymbol{Q_P}$ and $\boldsymbol{2Q_P}$ yields $Q_P^x = 0.117, Q_P^y = 0.129$; $2Q_P^x = 0.231, 2Q_P^y = 0.237$; $\delta Q_P^x = 0.020, \delta Q_P^y = 0.020$; and $\delta 2Q_P^x = 0.034, \delta 2Q_P^y = 0.035$. (Inset) $|\widetilde{\delta g}(\boldsymbol{q}, 30\text{ meV})|$. (**C** and **D**) As in (A) and (B) but at $E = -30$ meV. Measurement yields are $Q_P^x = 0.115, Q_P^y = 0.128$; $2Q_P^x = 0.239, 2Q_P^y = 0.235$; $\delta Q_P^x = 0.020, \delta Q_P^y = 0.020$; and $\delta 2Q_P^x = 0.039, \delta 2Q_P^y = 0.045$. (Inset) $|\widetilde{\delta g}(\boldsymbol{q}, -30\text{ meV})|$. The *s*-symmetry field-induced $N(\boldsymbol{r})$ modulations at $\boldsymbol{Q_P}$ and $2\boldsymbol{Q_P}$ are almost perfectly particle-hole symmetric [(B) and (D), insets] in the sense that $N(\boldsymbol{r}, E > 25\text{ meV}) = N(\boldsymbol{r}, E < -25\text{ meV})$ for these two wave vectors. (**E**) Fourier transform amplitude, $|\widetilde{\delta\Delta}(\boldsymbol{q})|$, of measured $\delta\Delta(\boldsymbol{r}) = \Delta(\boldsymbol{r}, 8.25\text{ T}) - \Delta(\boldsymbol{r}, 0)$ [(*44*), section 7]. The observed peaks revealing field-induced gap modulation occur at points indistinguishable from $\boldsymbol{Q_P}$. The peak along the (1, 1) direction occurs at the wave vector of the crystal supermodulation, where a modulation-induced PDW has long been identified. (**F**) Schematic representation of a bidirectional PDW with a *d*-symmetry form factor induced within a vortex halo that is consonant with the data in this work when considered in the context of vortex halo theory (*5*, *22*, *43*).

they are not inconsistent with an admixture of *s*-symmetry and *d*-symmetry components in the PDW order parameter. However, these modulations may also represent a field-induced version of the unidirectional *d*-symmetry form factor $N(\boldsymbol{r}, E)$ modulation observed in zero field (*45*).

But the predominant phenomena detected are the two sets of *s*-symmetry form factor modulations at $|\boldsymbol{Q_P}| \approx 1/8$ and $|2\boldsymbol{Q_P}| \approx 1/4$ (Fig. 4, A to D, red). Moreover, after subtraction of a smooth background, the widths δq of all $|\boldsymbol{Q_P}| \approx 1/8$ peaks are close to half of the $|2\boldsymbol{Q_P}| \approx 1/4$ peaks, as determined quantitatively by fitting as shown in Fig. 4, A to D. Averaged over the two directions (1, 0) and (0, 1) and energies $E = \pm 30$ meV, we found that $\delta(2\boldsymbol{Q_P}) = (1.8 \pm 0.2)\delta(\boldsymbol{Q_P})$ as expected for a field-induced PDW (Fig. 1) (*5*, *22*, *43*). As additional evidence of a PDW, we searched for energy gap modulations in measured $\Delta(\boldsymbol{r}) = \Delta_{SC} + \Delta_P \cos(\boldsymbol{Q_P} \cdot \boldsymbol{r})$. Generally, in superconductivity studies, the empirical $\Delta(\boldsymbol{r})$ is defined as half the energy separation of the coherence peaks in $N(\boldsymbol{r}, E)$ (Fig. 2B, horizontal arrow), so that field-induced changes to $\Delta(\boldsymbol{r})$ would here be defined as $\delta\Delta(\boldsymbol{r}) = \Delta(\boldsymbol{r}, 8.25\ T) - \Delta(\boldsymbol{r}, 0)$ [(*44*), section 7]. When measured, this $\delta\Delta(\boldsymbol{r})$ yields a Fourier transform $\delta\widetilde{\Delta}(\boldsymbol{q})$, as shown in Fig. 4E. This exhibits evidence for a field-induced energy-gap modulation at $\boldsymbol{Q_P}$ and not at $2\boldsymbol{Q_P}$, as would be expected specifically for a primary field-induced PDW at $\boldsymbol{Q_P}$.

Taken together, the results shown in Figs. 3 and 4 indicate that in $Bi_2Sr_2CaCu_2O_8$, a field-induced PDW state emerges within the halo region surrounding each quantized vortex core. The principal experimental signatures are two sets of $N(\boldsymbol{r})$ modulations occurring at $\boldsymbol{Q_P}$ and $2\boldsymbol{Q_P}$, both being particle-hole symmetric, both exhibiting principal amplitude with *s*-symmetry form factor, with the amplitude of $2\boldsymbol{Q_P}$ modulations decaying twice as rapidly as that of $\boldsymbol{Q_P}$ and with an apparently bidirectional structure, as shown schematically in Fig. 4F [(*44*), section 8]. These phenomena occur in an energy range $25 < |E| < 45$ meV, as might be expected theoretically for an $8a_0$ periodic PDW with energy gap magnitude Δ_P^Q occurring within that range. Several major implications stem from these observations. First and foremost, the primary state induced by high magnetic fields in the superconducting phase of cuprates is inferred to be a PDW with wave vector $\boldsymbol{Q_P}$, accompanied by secondary charge modulations at $\boldsymbol{Q_P}$ and $2\boldsymbol{Q_P}$. Second, the $8a_0$ periodicity points toward a strong correlation-driven microscopic mechanism for the PDW (*6*–*11*), in which case the form factor is generally predicted to have a *d*-symmetry (Fig. 4F). Third, because the PDW is generated by increasing magnetic field, our data imply that the high-field state of cuprates might itself be a PDW state (*4*), and if so, it is likely phase fluctuating and intertwined with additional CDW components. Last, putting all such conjectures aside, we emphasize that the experimental observations reported in Figs. 3 and 4 are in good, detailed, and quantitative agreement with theoretical models (*5*, *22*, *43*, *44*) for a primary PDW with wave vector $\boldsymbol{Q_P}$ induced within the cuprate vortex halo, which generates secondary CDWs at $\boldsymbol{Q_P}$ and $2\boldsymbol{Q_P}$.

REFERENCES AND NOTES

1. P. Fulde, R. A. Ferrell, *Phys. Rev.* **135** (3A), A550–A563 (1964).
2. A. I. Larkin, Y. N. Ovchinnikov, *Sov. Phys. JETP* **20**, 762–769 (1964).
3. E. Berg *et al*., *Phys. Rev. Lett.* **99**, 127003 (2007).
4. P. A. Lee, *Phys. Rev. X* **4**, 031017 (2014).
5. D. F. Agterberg, J. Garaud, *Phys. Rev. B* **91**, 104512 (2015).
6. A. Himeda, T. Kato, M. Ogata, *Phys. Rev. Lett.* **88**, 117001 (2002).
7. M. Raczkowski, M. Capello, D. Poilblanc, R. Fr'esard, A. M. Oleś, *Phys. Rev. B* **76**, 140505 (2007).
8. K.-Y. Yang, W. Q. Chen, T. M. Rice, M. Sigrist, F.-C. Zhang, *New J. Phys.* **11**, 055053 (2009).
9. F. Loder, A. P. Kampf, T. Kopp, *Phys. Rev. B* **81**, 020511 (2010).
10. P. Corboz, T. M. Rice, M. Troyer, *Phys. Rev. Lett.* **113**, 046402 (2014).
11. R.-G. Cai, L. Li, Y.-Q. Wang, J. Zaanen, *Phys. Rev. Lett.* **119**, 181601 (2017).
12. Q. Li, M. Hücker, G. D. Gu, A. M. Tsvelik, J. M. Tranquada, *Phys. Rev. Lett.* **99**, 067001 (2007).
13. E. Berg, E. Fradkin, S. A. Kivelson, *Nat. Phys.* **5**, 830–833 (2009).
14. E. Berg, E. Fradkin, S. A. Kivelson, J. M. Tranquada, *New J. Phys.* **11**, 115004 (2009).
15. C. Pépin, V. S. De Carvalho, T. Kloss, X. Montiel, *Phys. Rev. B* **90**, 195207 (2014).
16. H. Freire, V. S. de Carvalho, C. Pépin, *Phys. Rev. B* **92**, 045132 (2015).
17. Y. Wang, D. F. Agterberg, A. Chubukov, *Phys. Rev. Lett.* **114**, 197001 (2015).
18. D. F. Agterberg, D. S. Melchert, M. K. Kashyap, *Phys. Rev. B* **91**, 054502 (2015).
19. M. Zelli, C. Kallin, A. J. Berlinsky, *Phys. Rev. B* **84**, 174525 (2011).
20. M. Zelli, C. Kallin, A. J. Berlinsky, *Phys. Rev. B* **86**, 104507 (2012).
21. M. R. Norman, J. C. S. Davis, *Proc. Natl. Acad. Sci. U.S.A.* **115**, 5389–5391 (2018).
22. Z. Dai, Y.-H. Zhang, T. Senthil, P. A. Lee, *Phys. Rev. B* **97**, 174511 (2018).
23. F. Yu *et al*., *Proc. Natl. Acad. Sci. U.S.A.* **113**, 12667–12672 (2016).
24. M. H. Hamidian *et al*., *Nature* **532**, 343–347 (2016).
25. T. Wu *et al*., *Nature* **477**, 191–194 (2011).
26. J. Chang *et al*., *Nat. Phys.* **8**, 871–876 (2012).
27. D. LeBoeuf *et al*., *Nat. Phys.* **9**, 79–83 (2012).
28. S. Blanco-Canosa *et al*., *Phys. Rev. Lett.* **110**, 187001 (2013).
29. T. Wu *et al*., *Nat. Commun.* **6**, 6438 (2015).
30. S. Gerber *et al*., *Science* **350**, 949–952 (2015).
31. J. Chang *et al*., *Nat. Commun.* **7**, 11494 (2016).
32. H. Jang *et al*., *Proc. Natl. Acad. Sci. U.S.A.* **113**, 14645–14650 (2016).
33. B. Vignolle, D. Vignolles, M.-H. Julien, C. Proust, *C. R. Phys.* **14**, 39–52 (2013).
34. S. E. Sebastian, C. Proust, *Annu. Rev. Condens. Matter Phys.* **6**, 411–430 (2015).
35. J. E. Hoffman *et al*., *Science* **295**, 466–469 (2002).
36. K. Matsuba *et al*., *J. Phys. Soc. Jpn.* **76**, 063704 (2007).
37. S. Yoshizawa *et al*., *J. Phys. Soc. Jpn.* **82**, 083706 (2013).
38. T. Machida *et al*., *Nat. Commun.* **7**, 11747 (2016).
39. S. A. Kivelson, D. Lee, E. Fradkin, V. Oganesyan, *Phys. Rev. B* **66**, 144516 (2002).
40. D. F. Agterberg, H. Tsunetsugu, *Nat. Phys.* **4**, 639–642 (2009).
41. J. D. Sau, S. Sachdev, *Phys. Rev. B* **89**, 075129 (2014).
42. M. Einenkel, H. Meier, C. P'epin, K. B. Efetov, *Phys. Rev. B* **90**, 054511 (2014).
43. Y. Wang *et al*., *Phys. Rev. B* **97**, 174510 (2018).
44. Materials and methods are available as supplementary materials.
45. M. H. Hamidian *et al*., *Nat. Phys.* **12**, 150–156 (2016).
46. M. J. Lawler *et al*., *Nature* **466**, 347–351 (2010).
47. J. C. Davis, Supporting data for "Magnetic-field Induced Pair Density Wave State in the Cuprate Vortex Halo" by S. D. Edkins *et al*., Harvard Dataverse (2019); doi: 10.7910/DVN/JDSN1W

ACKNOWLEDGMENTS

We acknowledge and thank D. Agterberg, P. Choubey, A. Chubukov, E. Fradkin, P. J. Hirschfeld, P. D. Johnson, D. H. Lee, P. A. Lee, C. Pepin, S. Sebastian, S. Todadri, J. Tranquada, and Y. Wang for helpful discussions, advice, and communications. We are grateful to S. A. Kivelson for crucial proposals on the complete set of PDW phenomena to search for within the vortex halo. **Funding:** S.U. and H.E. acknowledge support from a Grant-in-Aid for Scientific Research from the Ministry of Science and Education (Japan); A.K. and K.F. acknowledge salary support from the U.S. Department of Energy, Office of Basic Energy Sciences, under contract DEAC02-98CH10886. E.-A.K. acknowledges support from the U.S. Department of Energy, Office of Basic Energy Sciences under award DE-SC0018946. S.S. acknowledges support under National Science Foundation under grant DMR- 1664842. J.C.S.D. acknowledges support from Science Foundation Ireland under award SFI 17/RP/5445 and from the European Research Council (ERC) under award DLV-788932. J.C.S.D., S.D.E., and M.H.H. acknowledge support from the Moore Foundation's EPiQS Initiative through grant GBMF4544. **Author contributions:** S.D.E., A.K., and M.H.H. carried out the experiments; K.F., H.E., and S.U. synthesized and characterized the samples; M.H.H., S.D.E., and K.F. developed and carried out analysis; S.S., M.J.L., and E.-A.K. provided theoretical guidance; A.P.M. and J.C.S.D. supervised the project and wrote the paper, with key contributions from S.D.E., K.F., and M.H.H. The manuscript reflects the contributions and ideas of all authors. **Competing interests:** The authors declare no competing financial interests. **Data and materials availability:** The data files for the results presented here are available at (*47*).

SUPPLEMENTARY MATERIALS

science.sciencemag.org/content/364/6444/976/suppl/DC1
Materials and Methods
Supplementary Text
Figs. S1 to S8
References (*48*–*58*)

5 February 2018; accepted 15 May 2019
10.1126/science.aat1773

Magnetic field–induced pair density wave state in the cuprate vortex halo

S. D. Edkins, A. Kostin, K. Fujita, A. P. Mackenzie, H. Eisaki, S. Uchida, Subir Sachdev, Michael J. Lawler, E.-A. Kim, J. C. Séamus Davis and M. H. Hamidian

Science **364** (6444), 976-980.
DOI: 10.1126/science.aat1773

Decoding the halo pattern

Magnetic fields can cause the formation of vortices in a superconductor. In cuprate superconductors, the vortex cores are surrounded by "halos," where the density of electronic states exhibits a checkerboard pattern. Edkins *et al.* used scanning tunneling spectroscopy to take a closer look into the halos. The results revealed that the patterns correspond to an exotic state called the pair density wave, in which the density of finite momentum Cooper pairs is spatially modulated.

Science, this issue p. 976